Wavelet Shrinkage for Enhanced Chemical Recognition in the Rough Surface Diffused Terahertz Spectra

Mahmoud E. Khani and M. Hassan Arbab
Stony Brook University, Stony Brook, NY, 11794 USA

***Abstract*— The rough surface scattering in the reflection-mode THz-TDS can result in inaccurate phase spectra, reduced signal to noise ratios, distorted or obscured resonant fingerprints, and the appearance of anomalous spectral artifacts. In this work, we demonstrate the implementation of a wavelet shrinkage technique for the retrieval of obscured resonant frequencies from the derivative of THz reflectivity of solid dielectric materials. We examine the robustness of this technique over controlled levels of rough surface scattering created using sandpapers of different grits on sample disks made from 4-aminobenzoic acid (PABA).**

I. INTRODUCTION

CHEMICAL recognition using the THz time-domain spectroscopy involves the identification of the unique resonant signatures in the dielectric functions of materials with vibrational or rotational molecular modes in the THz region. Considering that many materials of interest are opaque or highly absorptive in the THz region, reflection geometry is preferred for noninvasive spectroscopic applications. In the solid dielectric materials with moderate absorption relative to dispersion, the derivative of reflectivity to frequency can reveal the characteristic resonant frequencies [1]. However, in the solid materials with wavelength-scale surface roughness, except for the resonant signatures with a large full width at half maximum, spectral artifacts induced by the rough surface scattering will dominate the derivative of reflectivity [2]-[4]. This phenomenon results in distorted or obscured resonant signatures. In this work, we present the implementation of a wavelet shrinkage technique for the retrieval of characteristic resonant signatures resolved by the scattered terahertz (THz) reflectivity of molecular crystals. In this implementation, wavelet decomposition scales associated with the resonant signatures are identified based on the second-order total variation of the wavelet coefficients. Additionally, wavelet coefficients at selected scales are modified using the phase function correction and wavelet hard thresholding. Reconstruction of the original spectrum from these modified wavelet coefficients yields the resonant signatures that are otherwise unrecognizable. We examine the robustness of this technique over controlled levels of rough surface scattering in spectroscopic targets made from crystallin materials such as 4-aminobenzoic acid (PABA).

II. RESULTS

The flowchart in Fig. 1 displays the signal processing steps required for the wavelet shrinkage of the derivative of the THz reflectivity. After finding the wavelet and scaling coefficients of the derivative spectrum using the pyramid algorithm shown in Fig. 2, we correct the phase distortions caused by the scaling and wavelet filters, $\tilde{g}_j(f)$ and $\tilde{h}_j(f)$, in each decomposition level [5], [6]. Next, we find the wavelet basis functions that better capture a material's absorption signatures, while we

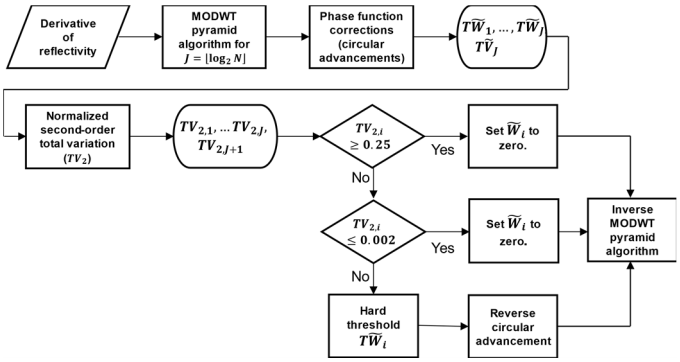

Fig. 1. The signal processing steps in the wavelet shrinkage of the derivative of the scattered THz reflectivity.

exclude those that are mainly associated with the scattering effects. For that purpose, we use the second-order total variation of the wavelet coefficients. For example, Fig. 3 compares the decomposition level-based second order total variation of the PABA samples with surface roughness ranging from grit 40 to grit 220. Figure 3 indicates that different levels of wavelet decomposition are well-separated based on this parameter, regardless of the surface roughness. We found that excluding the decomposition levels whose second-order total variation accounts for more than 25% or less than 0.2% of the total second-order total variation in the wavelet domain prior to wavelet shrinkage can significantly improve the results. For the remaining levels, we perform wavelet shrinkage by defining noise and scattering intervals for selecting a threshold. These intervals should be selected carefully to avoid any overlap with the resonant frequencies. Here, we found that using a 200-GHz spectral window centered at 300 GHz and a 200-GHz spectral window centered at 1.7 THz yields the best results.

Figure. 4(a) illustrates the schematic of the reflection THz-TDS apparatus for the measurement of the rough-surface

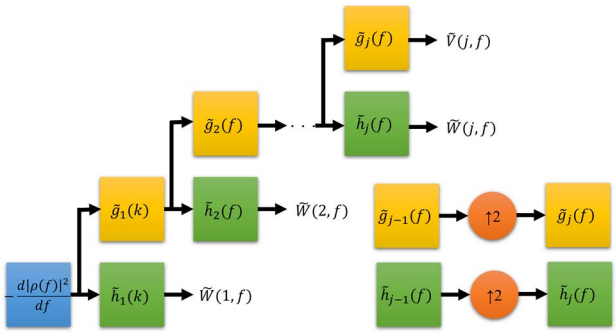

Fig. 2. The pyramid algorithm for computing the wavelet and scaling coefficients of the derivative of THz reflectivity $|\rho(f)|^2$ based on the maximal overlap discrete wavelet transform (MODWT). The $\tilde{g}_j$ *and* $\tilde{h}_j$ represent the jth-level scaling and wavelet filters [4].

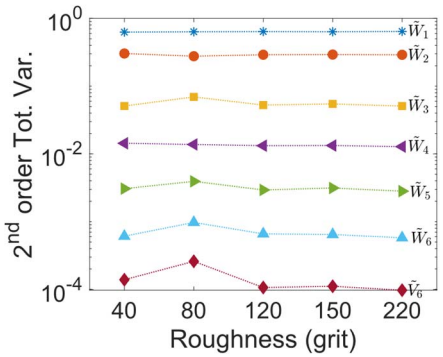

Fig. 3. The level-based second order total variation for the PABA samples with surface roughness ranging from grit 40 - 220. At each roughness level, these values are normalized by the total second order total variation in the wavelet domain. Therefore, their summation equals to one.

scattered THz fields in both specular and off-specular directions. The detection arm composed of two TPX50 lenses and a detector photoconductive antenna is mounted on a rotating rail, which pivots around the center axis of the sample to collect the scattered fields at different detection angles. Figure 4(b) exhibits the PABA extinction spectrum measured using transmission THz-TDS from a sample disk with grit 220 surface roughness. The red arrows point to the PABA resonant frequencies at 0.6, 0.8, 1.29, and 1.54 THz. Figure 4(c) illustrates the derivative of the THz reflectivity measured using the setup shown in Fig. 4(a) at the detection angle $\theta_r = 35^\circ$ (the specular direction). In Fig. 4(c), the red arrows point to the PABA resonant frequencies at 0.6 and 0.8 THz, while the blue circles delineate the spectral peaks caused by the scattering effects. Obviously, the PABA's higher-frequency resonances at 1.29 and 1.54 THz are obscured by the scattering effects. However, as it is shown in Fig. 4(d), the outcome of the proposed wavelet shrinkage technique applied to the signal shown in Fig. 4(c) yields all the PABA's resonant frequencies,

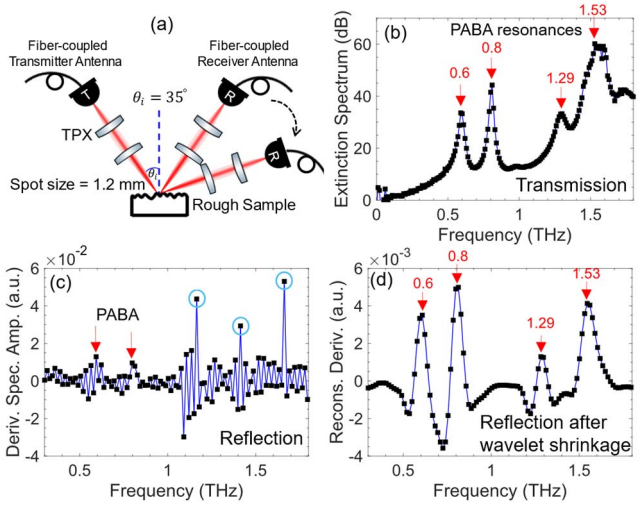

Fig. 4. (a) The schematic of the apparatus for measurement of the surface-reflected THz fields scattered to specular and off-specular directions, (b) the extinction spectrum of a PABA sample measured using transmission THz-TDS, (c) derivative of the reflectivity measured in reflection from a PABA sample grit 220 rough surface, (d) the outcome of the wavelet shrinkage of the derivative signal shown in (c)..

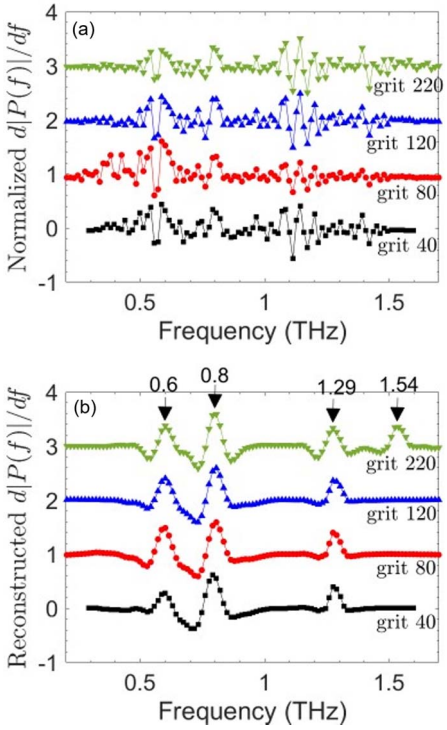

Fig. 5. The experimental results of the proposed wavelet shrinkage technique. (a) The derivative of the specular reflectivity from PABA samples with grit 40, 80, 120, and 220 surface roughness, (b) the wavelet shrinkage outcomes of the PABA reflectivities shown in (a).

even those masked by the scattering artifacts.

To further illustrate the robustness of the proposed wavelet shrinkage technique to more sever surface roughness levels, Fig. 5 exhibits the results obtained from the wavelet shrinkage of PABA samples with grit 40, 80, 120, and 220 surface roughness. Clearly, at all four roughness levels, in the derivative of the reflectivity, the higher-frequency resonances are obscured by the scattering effects. However, Fig. 5(b) illustrates that in the wavelet shrinkage outcome, the features at resonant frequencies appear as local maxima. Moreover, at grit 220, all the resonances at 0.6, 0.8, 1.29, and 1.54 THz are identified explicitly. Likewise, at more severe roughness levels, down to grit 40, resonances at 0.6, 0.8, and 1.29 are still explicitly identifiable. Comparing the results shown in Figs. 5(a) and 5(b) reveals that the wavelet shrinkage technique can reliably extract the resonant frequencies, even at extremely scattering scenarios.

REFERENCES

[1]. H. Zhong, A. Redo-Sanchez, and X.-C. Zhang, *Opt. Express,* vol. 14, pp. 9130-9141, 2006.

[2]. S. Schecklman, L. M. Zurk, S. Henry, and G. P. Kniffin, *J. Appl. Phys.*, vol. 109, pp. 094902, 2011.

[3]. M. H. Arbab, D. P. Winebrenner, E. I. Thorsos, and A. Chen, in *Proc. SPIE* 7601, San Francisco, CA, USA, 2010, pp. 760106-1–760106-7.

[4]. M. H. Arbab, D. P. Winebrenner, E. I. Thorsos, and A. Chen, *Appl. Phys. Lett.*, vol. 97, pp. 181903, 2010.

[5]. M. Ebrahimkhani and M. H. Arbab, in *2018 43rd International Conference on Infrared, Millimeter, and Terahertz Waves (IRMMW-THz)*, Nagoya, 2018, pp. 1-2.

[6]. M. E. Khani, D. Winebrenner and H. Arbab, in *IEEE Trans. Terahertz Sci. Technol.*, doi: 10.1109/TTHZ.2020.2997595.